Terahertz spectroscopic evidence of low-energy excitations in $NdNiO_3$

Rakesh Rana,[1,2] Parul Pandey,[1,2] V. Eswara Phanindra,[1] S. S. Prabhu,[3] and D. S. Rana[1,*]

[1]*Department of Physics, Indian Institute of Science Education and Research (IISER) Bhopal, Madhya Pradesh, 462066, India*

[2]*Institute of Ion Beam Physics and Materials Research, Helmholtz-Zentrum Dresden-Rossendorf, Bautzner Landstrasse 400, 01328 Dresden, Germany*

[3]*Department of Condensed Matter Physics and Material Sciences, Tata Institute of Fundamental Research, Mumbai 400 005, India*

(Received 1 May 2016; revised manuscript received 20 December 2017; published 16 January 2018)

The charge-density waves (CDW) in the framework Landau theory are visualized to manifest in complex $RNiO_3$ (R = rare-earth) nickelates in which the structure controls the incipient charge order in the weak localization limit. Any consequent effect demonstrating these nickelates in the rare category of CDW conductors with controlled charge-lattice interactions has been elusive so far. Employing terahertz time-domain spectroscopy along selective crystal axes, we present evidence of the CDW in epitaxial strain-modulated crystal structures of prototypical $NdNiO_3$. A finite peak structure at 5 meV in the terahertz conductivity displays all the characteristics of a CDW condensate in (110)- and (111)-oriented $NdNiO_3$ thin films. Contrasting charge dynamics of collective CDW mode and Drude conductivity emerging across dissimilar orientations helps disentangle charge ordering from the metal-insulator transition and establish a structure-property cause-effect relationship which may propose novel attributes in emerging oxide electronics.

DOI: 10.1103/PhysRevB.97.045123

I. INTRODUCTION

The correlated electrons which lower their energy and open a gap at the Fermi level form the most fascinating low-energy condensed-matter phases of collective transport, namely, the superconductivity, charge-density waves (CDW), and spin-density waves (SDW). The CDW originate from the real-space modulation of electronic charge densities pinned to their underlying lattice and are a unique source of collective excitations and collective charge transport [1–3]. They were originally found in low-dimensional systems, as attributed to the ease of formation of modulated charge densities and weak electron-phonon coupling in such systems [1]. Interestingly, these criteria are also satisfied by several high-dimensional correlated systems which, however, have rarely shown the CDW phases. Among them, high-temperature superconductors and manganites are the only systems which exhibit CDW resonance, and the impact of these limited observations has been decisive in resolving some key fundamental issues [4–8].

The rare-earth $RNiO_3$ (R = La-Lu) class of nickelates have attracted much attention both for their fundamental and technological fascinating attributes. In these systems, a combination of charge disproportionation and Fermi surface nesting can be envisaged as a precursor for the manifestation of the CDW [9–23]. The interplay of charge transfer and Mott physics presents a challenge to understand the charge/spin instabilities associated with insulator-metal (I-M) transition and complex magnetic order in these systems, whereas their heteroepitaxy-induced quantum criticality holds enormous potential for emerging oxide electronics [9–14,18]. Recently, the conjunction of quenched disorder and strain-induced modulation of the electrical properties and engineering of new phases was also observed [24]. Among all, the $NdNiO_3$ (NNO) is a unique system as it exhibits both the I-M transition and the E-type antiferromagnetic (AFM) order simultaneously at 205 K [15]. The Landau theory explains its magnetic structure in the framework of the nested SDW system, which induces the charge order (CO) as a secondary effect [19,20]. This CO has two characteristics, namely, its magnitude is directly proportional to the degree of orthorhombicity, and it ceases to exist in tetragonal/cubic symmetries [19,20]. In a different study, the density- and dynamic density-functional theories emphasized that large correlations in heavy rare-earth nickelates can quench the CO [25]. This, in conjunction with Landau theory, suggests that the charge disproportionation in nickelates may well exist within the weak correlations/localization limit, in which case it may condense into a rare CDW mode of collective transport. This mode, if detected, will provide a fresh paradigm to the underlying physics of nickelates and can be a source of novel functionalities to the emerging electronics based on them. However, any experimental demonstration of this phenomenon of CDW and understanding of its emergence along a selective crystal axis is much desired yet elusive so far. Here we have employed terahertz (THz) time-domain spectroscopy (TDS) on epitaxial strained NNO films along dissimilar orientations and show that a crossover from a CDW mode for (110)- and (111)-oriented films to a pure Drude-like conductivity manifests for (100)-oriented NNO films.

II. EXPERIMENTAL DETAILS

The bulk NNO has a $GdFeO_3$-type *Pnma* structure with lattice parameters as $a_o = 5.377$ Å, $b_o = 5.402$ Å, and $c_o = 7.608$ Å [26]. These orthorhombic lattice parameters can be related to their pseudocubic lattice constants as follows: $a_{pc} =$

*dsrana@iiserb.ac.in

 ©2018 American Physical Society

$b_{pc} = \sqrt{(a_o^2 + b_o^2)}/2 = 3.81$ Å, $c_{pc} = c_o/2 = 3.804$ Å, where subscripts *pc and o* refer to pseudocubic and orthorhombic notations, respectively. The NNO films were abbreviated in the form $(100)_{240\text{nm}}$, which refers to the film $(orientation)_{\text{thickness}}$. Also, $(001)_{pc}$ and $(111)_{pc}$ planes in pseudocubic notation are referred to as $(110)_o$ and $(101)_o$ planes in orthorhombic notations, respectively [27]. The NNO epitaxial thin films with two thicknesses of 240 nm and 35 nm were deposited using pulsed-laser deposition technique on $LaAlO_3$ (LAO) substrate along each of $(100)_{pc}$,$(110)_o$, and $(111)_{pc}$ orientations. The deposition was carried out using a 248 nm KrF excimer laser at a repetition rate of 4 Hz and with a laser fluence of 1.5 J/cm^2. The substrate was kept at a temperature of 700 °C. An O_2 pressure of 35 Pa was maintained during deposition, and postdeposition annealing of the films was carried out at 1 kPa of O_2 for 5 min. The thickness of the NNO films was measured using a Dektak XT Advanced surface profiler. The high-resolution x-ray diffraction measurements of all the NNO films were performed on a PANalytical Empyrean. Resistivity measurements were performed using a standard four-probe resistivity method on a Physical Property Measurement System, Quantum Design, USA. THz-TDS data in the range from 5 to 300 K were collected on a photoconductive (LT-GaAs) antenna-based TERA K-8 spectrometer from Menlo Systems GmbH (Germany) equipped with a cryostat JANIS (SHI-4-5) cryostat. The THz beam was passed from both the NNO sample and LAO bare substrate (used as reference) at different temperatures from 5 to 300 K. The amplitude and phase information of the NNO thin films was deduced using the fast Fourier transform of the transmitted THz pulse. After solving Fresnel's equations, we obtain a complex refractive index $\tilde{\varepsilon}(\omega) = \varepsilon_a(\omega) + i\varepsilon_b(\omega)$ from which the real part of optical conductivity can be deduced using the relation $\sigma(\omega) = \varepsilon_o\omega\varepsilon_b(\omega)$; here ε_o is the permittivity of free space [8].

III. RESULTS AND DISCUSSION

A. Structure and transport of $NdNiO_3$ thin films

The association of CDW with structure in simplistic form can be visualized from Figs. 1(a) and 1(b). All the NNO films are phase pure as no traces of impurity phases may be found in the x-ray diffraction θ-2θ scan (Fig. 2). The amount of strain in the NNO films was ascertained by recording reciprocal space maps (RSM) around asymmetric substrate peaks as shown in Fig. 1(c). It may be seen that the $(110)_{240\text{nm}}$ NNO film is relaxed, as the NNO film peak reflection and the LAO substrate reflection do not lie along the same pseudomorphic line. However, for the $(110)_{35\text{nm}}$ NNO film, the film peak and substrate peak occur along the same pseudomorphic line, suggesting thinner films to be strained, i.e., having the same in-plane parameter as that of the LAO substrate [Fig 1(c)]. Further, the RSM data indicate the $(110)_o$ and $(111)_{pc}$ NNO films to be orthorhombic and $(100)_{pc}$ NNO film to be tetragonal (Table I; for detailed RSM scans see Supplemental Material S1) [28]. The effect of strain along different crystal orientations is well established to stabilize the CO state [29]. All the NNO samples exhibit first-order insulator-metal (*I-M*) transition [Fig. 1(d)], with a transition temperature $(T_{I-M}) \sim 150$ K lower-compared to the bulk (~205 K). A higher resistive state

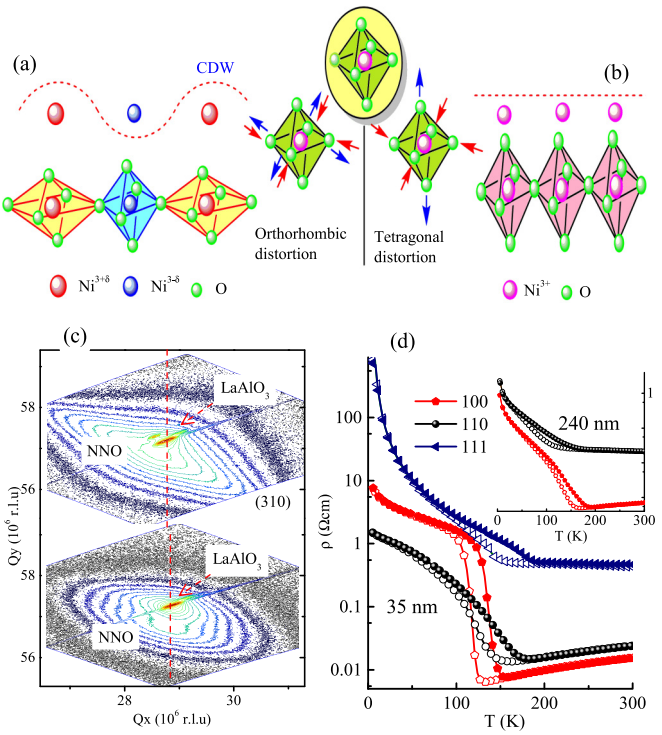

FIG. 1. Simplistic structure of $\langle NiO_6 \rangle$ octahedral. (a) An orthorhombic distortion leading to charge modulation, resulting in a CDW formation. (b) A tetragonal distortion leads to Drude-like conductivity. (c) High-resolution reciprocal space maps showing relaxed (upper) and strained NNO film across (110) orientation for asymmetric (310) reflection. (d) Resistivity (ρ) versus temperature (T) behavior of NNO films where solid and open symbols depict heating and cooling runs, respectively.

was obtained for thin $(111)_{35\text{nm}}$ film as compared to $(100)_{35\text{nm}}$ and $(110)_{35\text{nm}}$ films [28,30]. Also, the quality of *I-M* transition varies with the crystal orientation for the 35 nm films, i.e., the *I-M* transition for $(100)_{35\text{nm}}$ becomes much sharper than that for $(110)_{35\text{nm}}$ and $(111)_{35\text{nm}}$, whereas it may be noted that the $(110)_{240\text{nm}}$ NNO film possesses a highest resistive state which is about two orders of magnitude larger than the $(100)_{240\text{nm}}$ film [inset, Fig. 1(d)]. It is noteworthy that although we observed *I-M* transition for all NNO films, however we found that the intrinsic driving mechanism shows contrasting behavior across different orientations and can be understood from the low-energy dynamic response.

B. THz-TDS measurements

The low-energy THz conductivity (σ) data for the NNO films were measured along different in-plane crystal axes. For instance, for $(100)_{pc}$ sample the THz electric field was parallel (//) to $\langle 001 \rangle$ axes, for $(110)_o$ sample // to $\langle 1\bar{1}0 \rangle$ axes, and for $(111)_{pc}$ sample // to $\langle 10\bar{1} \rangle$ axes, presented in Figs. 3(a) and 3(b). These data show two types of qualitative features in σ-E (E is THz photon energy) spectra, namely, a finite peak structure in one set of NNO thin films and the Drude conductivity in another set of films. The $(110)_{240\text{nm}}$, $(110)_{35\text{nm}}$, and $(111)_{35\text{nm}}$ exhibit a pronounced peaklike structure in σ-E spectra at ~5−6 meV [Fig. 3(a) and Supplemental Material

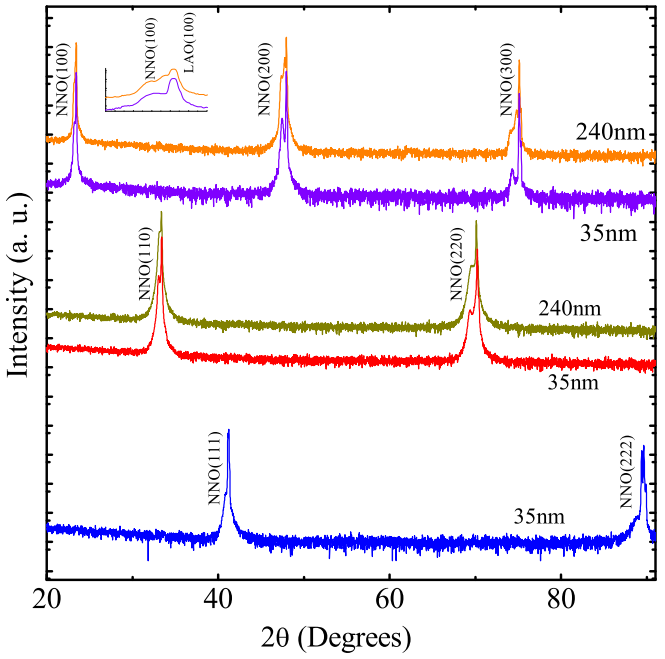

FIG. 2. X-ray diffraction of $NdNiO_3$ films across various orientations of $LaAlO_3$ substrate.

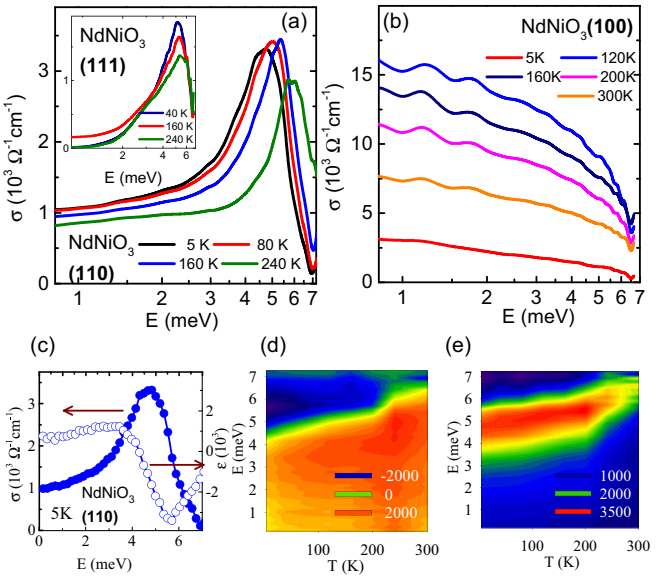

FIG. 3. The optical conductivity (σ) versus THz photon energy (E) for (a) inset for $(111)_{35nm}$ and $(110)_{240nm}$ and (b) for $(100)_{35nm}$ NNO films, respectively. (c) Dielectric dispersion for (110)-oriented film at 5 K. (d) Dielectric constant and (e) conductivity at various temperatures.

Fig. S3] [28]. In contrast, the σ-E spectra of both $(100)_{240nm}$ and $(100)_{35nm}$ films, sans a peak structure, are reminiscent of a Drude-like conductivity [Fig. 3(b) and Supplemental Material Fig. S3(d)] [28]. The observed peak in σ-E spectra for $(110)_o$ and $(111)_{pc}$ films possesses all the typical attributes of the CDW mode, for instance, a resonance frequency in the range of ∼1−8 meV, values of σ and dielectric constant (ε) on the order of 10^3, and a dielectric dispersion [a zero crossing in ε at the peak σ frequency as shown in Fig. 3(c)] [1,7,8,29]. However, it is imperative to discuss the possibility of phonon modes as they also start emerging below the *I-M* transition of NNO [29]. In this context, the phonon vibrations of the Nd ion against the oxygen octahedral manifests at ∼23 meV, a breathing phonon ∼62 meV, vibrational mode ∼85 meV, and the overtone intensities occurs at ∼130 meV [31]. The observed CDW mode in NNO is much below ∼5−6 meV, although the presence of optical phonons is at much higher frequencies but can get strongly renormalized by the epitaxial strain in thin films. However, the energy range of softening of these phonon energies should be too large and would affect the first few layers, while we are probing the macroscopic properties using THz radiation in transmission mode. For the perovskite manganites, another possibility of far-infrared active mode was noted due to Brillouin-zone folding [32]. However, σ of NNO films is about two orders of magnitude larger and one peak in σ-E spectra for NNO films is observed compared to two peak structures which attest to the CDW excitations in $(110)_o$ and $(111)_{pc}$ samples.

The collective excitations associated with the CDW are called amplitudon and phason, respectively. The amplitudon mode is Raman-active and corresponds to the variation in CDW amplitude without displacement of the charge density relative to the lattice, and the phason mode is associated with the displacement of the electronic charge density relative to the lattice ions [1]. To assign the CDW mode, recent studies have indicated that amplitudon mode manifests around ∼7 meV and the phason mode ∼1 meV [33,34]. The possibility of the amplitudon mode in the NNO can be discarded as the amplitudon mode exhibits strong temperature dependence and should completely vanish above the metal-insulator transition. Given this, the CDW mode in NNO can be ascribed to the pinned phason mode, although we observe a slightly higher pinning frequency. It is well known that lattice imperfections either due to strain or upon chemical doping can cause the shift in the pinning frequency of this phason mode [28,34]. This can also be seen in CDW mode for NNO films as a slightly different

TABLE I. Lattice constant of $NdNiO_3$ thin films on $LaAlO_3$ substrate.

Sample $(orientation)_{thickness}$	In-plane lattice constant a (Å)/ (in-plane axes)		In-plane lattice constant b (Å)/ (in-plane axes)		Out-of-plane lattice constant c (Å)
$(100)_{240nm}$	3.83	[001]	3.831	[010]	3.804
$(110)_{240nm}$	3.785	[001]	3.814	$[1\bar{1}0]$	3.807
$(100)_{35nm}$	3.79	[001]	3.790	[010]	3.833
$(110)_{35nm}$	3.79	[001]	3.805	$[1\bar{1}0]$	3.83
$(111)_{35nm}$	3.79	$[11\bar{2}]$	3.799	$[1\bar{1}0]$	3.81

pinning frequency was observed for different samples. Further, for a sample with better crystallinity, the CDW resonance for NNO at a lower frequency of ∼3 meV was also noted (see text and Supplemental Material Fig. S4) [28,31]. Further, the CDW mode is directly linked to the strength/range of the CO correlations and can give subtle information about the nature of CO. We observed that the CDW peak for $(110)_{240nm}$ film is pronounced as compared to $(111)_{35nm}$ and $(110)_{35nm}$ films; this suggests that the CO state for the $(110)_{240nm}$ film is more robust as compared to $(111)_{35nm}$ and $(110)_{35nm}$ film (Supplemental Material Fig. S5) [28]. The CDW peak becomes shallower above the *I-M* transition, and its occurrence may be ascribed to the short-range CO fluctuations noted in the paramagnetic (PM) phase of NNO (Supplemental Material Fig. S3) [28,35].

C. Drude-Lorentz analysis of optical conductivity

The optical conductivity of NNO films was modeled with the phenomenological Drude-Lorentz (D-L) model using the equation

$$\sigma(\omega) = \frac{1}{4\pi}\frac{\Gamma_d \omega_{PD}^2}{{\Gamma_d}^2 + \omega^2} + \frac{1}{4\pi}\frac{S_n^2 \omega^2 \gamma_n}{\left(\omega_n^2 - \omega^2\right)^2 + \omega^2 \gamma_n^2}, \quad (1)$$

where the fitting parameter ω_{PD} is the Drude plasma frequency, Γ_d is the Drude scattering rate, ω_n is the center peak frequency, γ_n is the width, and S_n^2 is the mode strength for the nth Lorentz harmonic oscillator [36]. The σ-E spectral data of $(110)_{240nm}$ and $(111)_{35nm}$ films show good agreement with the D-L model at various temperatures as shown in Figs. 4(a) and 4(b) and fitted values are given in Table II. However, a marginal deviation at low temperatures indicated by the red arrow is noticeable, indicating a slight asymmetry of the CDW peak (Supplemental Material Fig. S3) [28,34,37]. This asymmetry may arise due to different pinning centers present in the NNO film and reduces as the temperature is increased from 5 to 150 K and nearly vanishes for 200 K for the $(110)_{240nm}$, as the $(100)_{240nm}$ and $(100)_{35nm}$ exhibit only Drude-like conductivity and their spectra fit well with the Drude part of the D-L model [Fig. 4(d)]. Further, our data of ε for $(110)_{240nm}$ also fit well with the generic CDW equation $\varepsilon(\omega) = \varepsilon_\infty + \omega_{PL}^2(\omega_{peak}^2 - \omega^2)/(\omega_{peak}^2 - \omega^2)^2 + \omega^2\Gamma^2$, where $\omega_{PL}, \omega_{peak}, \varepsilon_\infty$, and Γ are the plasma frequency, peak frequency of the CDW mode, the dielectric constant of the bound electron at infinity, and scattering rate, respectively [Fig. 4(c)] [1,8].

TABLE II. Drude-Lorentz fitting parameters for optical conductivity of $NdNiO_3$ thin films.

Sample	Temperature (K)	ω_{PD}	Γ_d	S_1	γ_n
$(110)_{240nm}$	5	272.8	4.6	254	1.79 ± 0.2
	120	307.6	6.2	256	1.87 ± 0.3
	240	454.4	8.6	236	2.13 ± 0.15
$(100)_{240nm}$	5	691.3	11.5		
	120	831.7	14.1		
	240	1062	15.5		

D. Scattering rate analysis and theoretical considerations for CDW emergence

For the CDW excitations, the scattering rate (Γ) versus temperature (T) should obey the relation $\Gamma(T) = \Gamma_o + AT^2$, where Γ_o is the $\Gamma(T \to 0\ \text{K})$ and A is the constant [Fig. 5(a) and the inset] [1,8]. We find that for $(110)_{35nm}$, $(110)_{240nm}$, and $(111)_{35nm}$ films with CDW excitations, the experimental data follow this equation below the *I-M* transition (∼150 K) [Fig. 5(a)]. The fitted values thus obtained are $\Gamma_o = 3.1$, 1.6, and 2.08 meV, while $A = 0.69$, 0.015, and 0.04 meV/K^2 for the $(110)_{35nm}$, $(110)_{240nm}$, and $(111)_{35nm}$, respectively. These values are in the similar range as of the classic 3d manganite CDW systems [8,29]. The CDW excitations in the NNO films can be associated with the opening of a pseudogap below the single-particle excitation spectrum. The values of gap Δ can be determined using a thermally activated hopping model

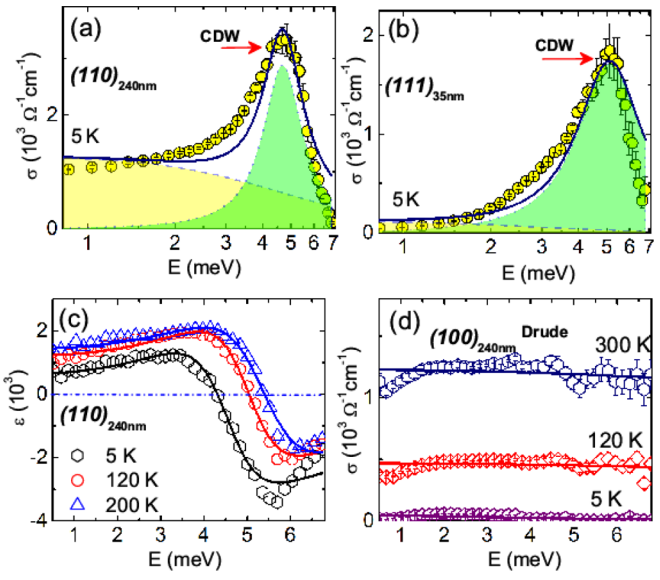

FIG. 4. Drude-Lorentz fitting. (a), (b) D-L fits for $(110)_{240nm}$ and $(111)_{35nm}$ NNO films, respectively. Here, symbols, solid red line, dotted line (with green shaded area), and dashed lines (with yellow shaded area) depict the experimental data, D-L fit, Lorentz contribution, and Drude contribution, respectively. (c) ε at various temperature for $(110)_{240nm}$. (d) Drude fitting (solid line) for $(100)_{240nm}$ film.

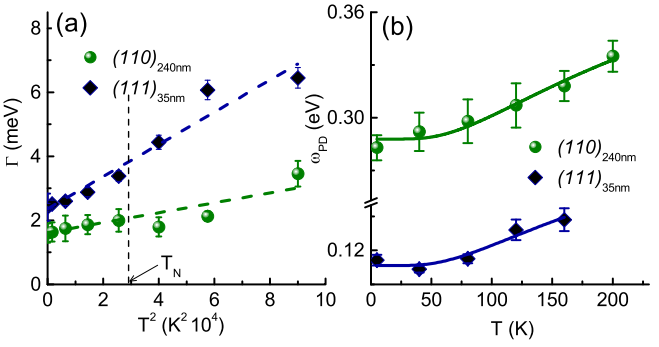

FIG. 5. Scattering rate analysis for CDW. (a) Scattering rate (Γ) versus the square of the temperature (T) for $(111)_{35nm}$ and $(110)_{240nm}$. Here, the dashed line is the fit and (b) shows the Drude plasma frequency (ω_{PD}) versus temperature; the solid line depicts the fit.

which can be suitably fit in the low-frequency range (i.e., 0.4 THz) of the optical conductivity data, where Drude carriers are more activated. For fitting the equation $\omega_{PD}(T)/\sigma(T) = A_o \exp[-\Delta/k_\beta T] + B$ was used, as shown in Fig. 5(b) (here A_o is a constant, Δ is the activation energy, k_β is the Boltzmann constant, and B is the nonzero offset) [38]. The values of Δ after fitting $\omega_{PD}(T)$ for $(110)_{35nm}$ is 24(±4) meV, $(110)_{240nm}$ is 25 ± 3 meV, and $(111)_{240nm}$ is 29 ± 6meV. These distinct values of Δ for NNO films may arise due to the difference in the quality of samples [39]. It is remarkable that the obtained values of Δ follow the standard BCS picture of the gap opening with $2\Delta \sim 3.5\, k_\beta T_N$; using this for bulk NNO, a $\Delta \sim 30$ meV for $T_N \sim 205$ K and a $\Delta \sim 22$ meV for a $T_N \sim 150$ K in the case of NNO films may be approximated [see Supplemental Material Fig. S2(b)] [18,28,30,40]. This is a strong indication of the electron-phonon coupling [41]. The values of Δ for NNO films are less than the measured SDW gap of ~200 meV using optical spectroscopy; however, they are in good agreement with a Δ of ~15 meV (using $T_N \sim 100$ K) and a Δ of ~44 meV found using Fourier transform infrared spectroscopy [9,11,42]. Our experimental values of Δ for NNO are suggestive of a BCS theory-based picture for the states near the Fermi level. Further, recent theoretical calculations and optical measurements also predict a Peierls-like gap to develop due to octahedral breathing distortion in the low-temperature monoclinic phase of the nickelates [43].

E. Spectral weight across different orientation for $NdNiO_3$

The spectral weight (SW) of the Lorentz and Drude part was calculated from the D-L fits to the experimental data. The SW can effectively track the charge redistribution due to the optical sum rule and can provide the valuable insights of the condensed (in the CDW phase) and uncondensed electrons (Drude carriers). The SW was deduced using the equation $SW = \int_{\omega 1}^{\omega 2} \sigma(\omega) d\omega$, where $\omega_1 = 0.5$ meV and $\omega_2 = 7$ meV are the upper and lower cutoff frequencies, respectively [7]. It may be seen that the Drude spectral weight (DSW) for $(110)_{240nm}$ and $(111)_{35nm}$ is nearly temperature independent [Fig. 6(a)]. However, for all other samples, it increases sharply in the vicinity of $T_{I-M} \sim 150$ K. As the 35-nm $(100)_{pc}$ films contain uncondensed Drude electrons only, their DSW is 2–4 times larger than that of other films which contain superimposed

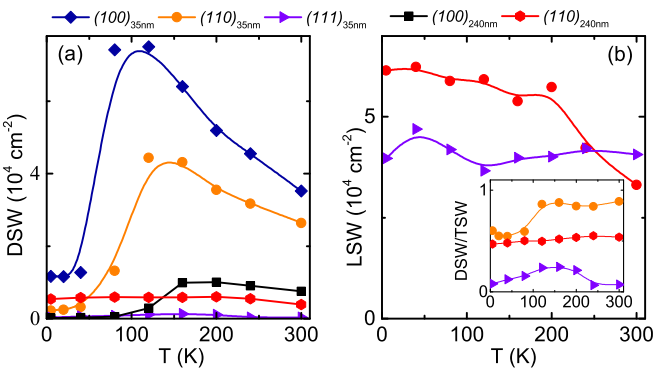

FIG. 6. Spectral weight across different orientations of $NdNiO_3$. Temperature dependence of (a) DSW and (b) LSW. The inset shows the ratio of DSW/TSW for NNO films.

CDW and Drude components [Fig. 6(a)]. The Lorentz spectral weight (LSW) for $(110)_{240nm}$ film keeps increasing and remains constant for $(111)_{35nm}$ at lower temperatures, which suggests more electrons gets condensed in the CDW phase for the former than the latter [Fig. 6(b)]. The Drude carrier concentration (N) was deduced from the Drude plasma frequency (ω_{PD}) using the relation $\omega_{PD}^2 = 4\pi N e^2/m^*$, where $m^* \sim 6\, m_o$ is the effective mass and m_o is the mass of the free electron (Supplemental Material Fig. S7) [28]. An N of the order of $\sim 10^{19}$ in the insulating and $\sim 10^{20}$ for metallic phase was obtained for $(100)_{35nm}$ and $(100)_{240nm}$ films. For $(110)_{240nm}$ film exhibiting CDW mode, the value of N varied from $\sim 10^{18}$ in the insulating state to $\sim 10^{19}$ in the metallic state, which is less than the $(100)_{pc}$-oriented films exhibiting the Drude behavior. Our calculated values of N are in a similar range to those obtained using infrared spectroscopy $\sim 10^{18}$ and less than the estimation of $N \sim 10^{22}$ assuming one electron per Ni site [12,31]. The reduction in N in the low-temperature phase may be associated with the setting of the unusual E-type AFM order, whereas the higher values of ω_{PD} above the I-M transition (Supplemental Material Fig. S7) indicate weaker electronic correlations in the PM phase [28].

The magnitude of the CDW peak and its presence and absence for the NNO films can be modulated by growing it across dissimilar orientations as the CDW peak shows up for $(110)_o$ and $(111)_{pc}$ films, being strongest in most distorted $(110)_{240nm}$ film while being absent for $(100)_{pc}$ films. As per Landau theory, two types of ground state were predicted for NNO, namely, a site-centered and bond-centered [19,20]. The former occurs in cubic/tetragonal structure, results in equal moments (Ni^{3+}) at all Ni sites, and does not induce the charge disproportionation and no CDW as observed for $(100)_{pc}$ films. This is analogous to NNO films in which the strain was viewed to be accommodated via Ni–O bond bending and stretching, precluding the charge-disproportionation of Ni in the ground state [44]. Thus, the I-M transition is purely SDW type and brings the relevance of the Mott physics to explain the insulating character of $(100)_{pc}$ NNO films. In contrast to $(110)_o$ and $(111)_{pc}$ NNO films, the bond-centered SDW is driven off-center and leads to charge disproportionation with $Ni^{3+\delta} - Ni^{3-\delta}$ ($\delta \sim 0.2$–0.5) as a secondary effect and the CDW mode [13,19,20].

Theoretical description of CDW as per Landau theory pointed toward the one-dimensional character and enhanced susceptibilities for NNO at the certain wave vectors leading to SDW/CDW formation [19,20]. This scenario is analogous to Peierl's idea of the CDW formation [1]. For our data, a gap value of $\Delta \sim 22$ meV for NNO suggests the localization of charges carriers and the electron-phonon coupling. To relate the gap opening with the nesting tendency of the Fermi surface, we define a quantity Φ as the ratio of DSW and total spectral weight (TSW) [inset, Fig. 6(b)] [36]. The Φ is a measure of the fraction of Fermi surface not affected by the CDW state, as a smaller (larger) Φ indicates the Fermi surface is largely gapped (ungapped). In the $(110)_{240nm}$ and $(111)_{35nm}$ film, a $\Phi \sim 0.5$ and $\Phi \sim 0.2$–0.3 suggest that nearly half of the Fermi surface is gapped for the former and more than half for the latter, respectively [Fig. 6(b)]. This imperfect nesting of the Fermi surface results from the electronic inhomogeneities in the region of coexisting metallic and insulating phases

below the *I-M* transition. Further, a $\Phi \sim 1$ for the $(100)_{pc}$-oriented NNO films suggests an ungapped Fermi surface, which lacks the CDW mode. Another key attribute of the CDW mode is its anisotropic character which is also observed (Supplemental Material text and Fig. S8) for $(110)_{240\text{nm}}$ film due to the directional character of the Ni, e_g orbital in NNO [7,19,20,28].

To summarize, we have presented the spectroscopic evidence of the CDW in the charge-disproportionate phase of $NdNiO_3$ highlighting the electron-lattice coupling in the weak localization limit. The precise control of the low-energy mode in nickelates may serve as a new channel of collective charge transport which can have potential implications in the emerging oxide electronics based on them.

ACKNOWLEDGMENTS

D.S.R. thanks the Science and Engineering Research Board (SERB), Department of Science and Technology (DST), New Delhi, for financial support under research Project No. EMR/2016/003598. Financial support from DST-FIST Project No. SR/FST/PSI-195/2014(C) is also thankfully acknowledged.

[1] G. Grüner, Rev. Mod. Phys. **60**, 1129 (1988).
[2] G. C. Milward, M. J. Calderón, and P. B. Littlewood, Nature (London) **433**, 607 (2005).
[3] S. Cox, J. Singleton, R. D. McDonald, A. Migliori, and P. B. Littlewood, Nat. Mater. **7**, 25 (2008).
[4] D. H. Torchinsky, F. Mahmood, A. T. Bollinger, I. Božović, and N. Gedik, Nat. Mater. **12**, 387 (2013).
[5] G. Coslovich, B. Huber, W. S. Lee, Y.-D. Chuang, Y. Zhu, T. Sasagawa, Z. Hussain, H. A. Bechtel, M. C. Martin, Z. X. Shen, R. W. Schoenlein, and R. A. Kaindl, Nat. Commun. **4**, 2643 (2013).
[6] Y. Uozu, Y. Wakabayashi, Y. Ogimoto, N. Takubo, H. Tamaru, N. Nagaosa, and K. Miyano, Phys. Rev. Lett. **97**, 037202 (2006).
[7] R. Rana, P. Pandey, D. S. Rana, K. R. Mavani, I. Kawayama, H. Murakami, and M. Tonouchi, Phys. Rev. B **87**, 224421 (2013).
[8] N. Kida and M. Tonouchi, Phys. Rev. B **66**, 024401 (2002).
[9] M. K. Stewart, J. Liu, M. Kareev, J. Chakhalian, and D. N. Basov, Phys. Rev. Lett. **107**, 176401 (2011).
[10] P. Ruello, S. Zhang, P. Laffez, B. Perrin, and V. Gusev, Phys. Rev. B **76**, 165107 (2007).
[11] T. Katsufuji, Y. Okimoto, T. Arima, Y. Tokura, and J. B. Torrance, Phys. Rev. B **51**, 4830 (1995).
[12] X. Granados, J. Fontcuberta, X. Obradors, Ll. Mañosa, and J. B. Torrance, Phys. Rev. B **48**, 11666 (1993).
[13] U. Staub, G. I. Meijer, F. Fauth, R. Allenspach, J. G. Bednorz, J. Karpinski, S. M. Kazakov, L. Paolasini, and F. d'Acapito, Phys. Rev. Lett. **88**, 126402 (2002).
[14] R. Scherwitzl, P. Zubko, I. G. Lezama, S. Ono, A. F. Morpurgo, G. Catalan, and J. M. Triscone, Adv. Mater. **22**, 5517 (2010).
[15] J. L. García-Muñoz, J. Rodríguez-Carvajal, and P. Lacorre, Phys. Rev. B **50**, 978 (1994).
[16] I. I. Mazin, D. I. Khomskii, R. Lengsdorf, J. A. Alonso, W. G. Marshall, R. M. Ibberson, A. Podlesnyak, M. J. Martinez-Lope, and M. M. Abd-Elmeguid, Phys. Rev. Lett. **98**, 176406 (2007).
[17] J. L. García-Muñoz, M. A. G. Aranda, J. A. Alonso, and M. J. Martínez-Lope, Phys. Rev. B **79**, 134432 (2009).
[18] J. Liu, M. Kargarian, M. Kareev, B. Gray, P. J. Ryan, A. Cruz, N. Tahir, Y.-D. Chuang, J. Guo, J. M. Rondinelli, J. W. Freeland, G. A. Fiete, and J. Chakhalian, Nat. Commun. **4**, 2714 (2013).
[19] S. Lee, R. Chen, and L. Balents, Phys. Rev. Lett. **106**, 016405 (2011).
[20] S. Lee, R. Chen, and L. Balents, Phys. Rev. B **84**, 165119 (2011).
[21] J. A. Alonso and J. L. García-Muñoz, Phys. Rev. Lett. **82**, 3871 (1999).
[22] J. Liu, M. Kareev, B. Gray, J. W. Kim, P. Ryan, B. Dabrowski, J. W. Freeland, and J. Chakhalian, Appl. Phys. Lett. **96**, 233110 (2010).
[23] V. Eswara Phanindra, S. Das, K. Santhosh Kumar, P. Agarwal, R. Rana, and D. S. Rana, Phys. Rev. B **95**, 085114 (2017).
[24] S. Das, V. Eswara Phanindra, S. S. Philip, and D. S. Rana, Phys. Rev. B **96**, 144411 (2017).
[25] H. Park, A. J. Millis, and C. A. Marianetti, Phys. Rev. Lett. **109**, 156402 (2012).
[26] J. Blasco, J. Gracia, F. J. Lazaro, and M. G. Proietti, J. Magn. Magn. Mater. **140/144**, 1813 (1995).
[27] S. Catalano, M. Gibert, V. Bisogni, F. He, R. Sutarto, M. Viret, P. Zubko, R. Scherwitzl, G. A. Sawatzky, T. Schmitt, and J. Triscone, APL Mater. **3**, 62506 (2015).
[28] See Supplemental Material at http://link.aps.org/supplemental/10.1103/PhysRevB.97.045123 for reciprocal space maps, transport measurements, Drude-Lorentz fitting, thermal evolution of CDW, terahertz data at 5 K, temperature dependence of optical conductivity and Drude plasma frequency, and directional properties of Ni-e_g orbitals of $NdNiO_3$ thin films.
[29] R. Rana, D. S. Rana, K. R. Mavani, I. Kawayama, H. Murakami, and M. Tonouchi, Appl. Phys. Lett. **101**, 252401 (2012).
[30] J. S. Zhou, J. Goodenough, and B. Dabrowski, Phys. Rev. Lett. **95**, 127204 (2005).
[31] N. Massa, J. Alonso, M. Martínez-Lope, and I. Rasines, Phys. Rev. B **56**, 986 (1997).
[32] T. Zhang, E. Zhukova, B. Gorshunov, D. Wu, A. S. Prokhorov, V. I. Torgashev, E. G. Maksimov, and M. Dressel, Phys. Rev. B **81**, 125132 (2010).
[33] H. Schäfer, V. V. Kabanov, M. Beyer, K. Biljakovic, and J. Demsar, Phys. Rev. Lett. **105**, 066402 (2010).
[34] L. Degiorgi and G. Grüner, Phys. Rev. B **44**, 7820 (1991).
[35] C. Piamonteze, H. C. N. Tolentino, A. Y. Ramos, N. E. Massa, J. A. Alonso, M. J. Martínez-Lope, and M. T. Casais, Phys. Rev. B **71**, 012104 (2005).
[36] M. Lavagnini, A. Sacchetti, L. Degiorgi, K. Y. Shin, and I. R. Fisher, Phys. Rev. B **75**, 205133 (2007).
[37] G. Mihaly, T. W. Kim, and G. Grüner, Phys. Rev. B **39**, 13009 (1989).
[38] C. S. Tang, B. Xia, X. Zou, S. Chen, H. W. Ou, L. Wang, A. Rusydi, J. X. Zhu, and E. E. M. Chia, Sci. Rep. **3**, 3513 (2013).
[39] A. Nucara, P. Maselli, P. Calvani, R. Sopracase, M. Ortolani, G. Gruener, M. C. Guidi, U. Schade, and J. García, Phys. Rev. Lett. **101**, 066407 (2008).

[40] M. Tinkham, *Introduction to Superconductivity*, 2nd ed. (McGraw-Hill, New York, 1996).

[41] M. Medarde, P. Lacorre, K. Conder, F. Fauth, and A. Furrer, Phys. Rev. Lett. **80**, 2397 (1998).

[42] S. J. Allen, A. J. Hauser, E. Mikheev, J. Y. Zhang, N. E. Moreno, J. Son, D. G. Ouellette, J. Kally, A. Kozhanov, L. Balents, and S. Stemmer, APL Mater. **3**, 62503 (2015).

[43] J. Ruppen, J. Teyssier, O. E. Peil, S. Catalano, M. Gibert, J. Mravlje, J. M. Triscone, A. Georges, and D. Van Der Marel, Phys. Rev. B **92**, 155145 (2015).

[44] J. Chakhalian, J. M. Rondinelli, J. Liu, B. A. Gray, M. Kareev, E. J. Moon, N. Prasai, J. L. Cohn, M. Varela, I. C. Tung, M. J. Bedzyk, S. G. Altendorf, F. Strigari, B. Dabrowski, L. H. Tjeng, P. J. Ryan, and J. W. Freeland, Phys. Rev. Lett. **107**, 116805 (2011).